Geophysical Research Letters

RESEARCH LETTER
10.1029/2019GL086767

# Direct Evidence for Fluid Pressure, Dilatancy, and Compaction Affecting Slip in Isolated Faults

B. Proctor[1,2], D. A. Lockner[2], B. D. Kilgore[2], T. M. Mitchell[3], and N. M. Beeler[2]

[1]Naval Surface Warfare Center, Crane, IN, USA, [2]U. S. Geological Survey, Menlo Park, CA, USA, [3]Department of Earth Sciences, University College London, London, UK

**Key Points:**
- Direct measurements of pore pressure show variations during nucleation and rupture using a miniature pressure transducer
- Fluids and intrinsic friction interact in controlling fault stability
- The effect of fluid pressure changes can exceed frictional variations predicted by the rate- and state-dependent friction laws

**Supporting Information:**
- Supporting Information S1

**Correspondence to:**
T. M. Mitchell,
tom.mitchell@ucl.ac.uk

**Citation:**
Proctor, B., Lockner, D. A., Kilgore, B. D., Mitchell, T. M., & Beeler, N. M. (2020). Direct evidence for fluid pressure, dilatancy, and compaction affecting slip in isolated faults. *Geophysical Research Letters*, *47*, e2019GL086767. https://doi.org/10.1029/2019GL086767

Received 23 DEC 2019
Accepted 23 JUN 2020
Accepted article online 24 JUN 2020



**Abstract** Earthquake instability occurs as a result of strength loss during sliding on a fault. It has been known for over 50 years that fault compaction or dilatancy may cause significant weakening or strengthening by dramatically changing the fluid pressure trapped in faults. Despite this fundamental importance, we have no real understanding of the exact conditions that lead to compaction or dilation during nucleation or rupture. To date, no direct measurements of pore pressure changes during slip in hydraulically isolated faults have been reported. We show direct examples of fluid pressure variations during nucleation and rupture using a miniature pressure transducer embedded in an experimental fault. We demonstrate that fluids not only are significant in controlling fault behavior but can provide the dominant mechanism controlling fault stability. The effect of fluid pressure changes can exceed frictional variations predicted by rate- and state-dependent friction laws, exerting fundamental controls on earthquake rupture initiation.

## 1. Introduction

Changes in pore fluid pressure directly affect fault stability for natural and induced earthquakes. In the brittle crust the standard expectation from the effective pressure law is that the fault shear strength, $\tau$, depends on pore pressure, $p$, as

$$\tau = \mu^{eff}\,(\sigma_n - p) = \mu^{eff}\,\sigma_n{}^{eff}, \tag{1}$$

where $\sigma_n$ is fault-normal stress and $\mu^{eff}$ is the coefficient of friction (Hubbert & Rubey, 1959; Terzaghi, 1936). Effective normal stress is defined as $\sigma_n{}^{eff} = \sigma_n - p$. Slip instability arises when the fault loses strength with slip, $\delta$, more rapidly than shear stress is elastically unloaded: $-\mathrm{d}\tau/\mathrm{d}\delta > k$. In the laboratory, elastic stiffness, $k$, is a characteristic of the test apparatus, the sample, or a combination of the two (Shimamoto et al., 1980). Accordingly, at constant applied normal stress, instability can arise when $\mathrm{d}p/\mathrm{d}\delta > k/\mu$. At undrained conditions (constant fluid mass), pore pressure changes occur when the pore volume or pore temperature changes; there are a number of mechanisms that do this. For instance, shear deformation of overcompacted fault zones produces dilatancy, reducing the pore pressure in an incompletely drained fault (Rice & Rudnicki, 1979; Segall et al., 2010; Segall & Rice, 1995) (dilatancy hardening). In low-permeability intact rock, dilatancy hardening can lead to delayed failure as $p$ drops and then recovers with influx of fluid from surrounding rock (Brantut, 2020; Stanchits et al., 2003). Conversely, shear of undercompacted material produces pore compaction (Mandl et al., 1977) that implies an increase in pore pressure (compaction weakening). At the elevated normal stresses and sliding velocities during earthquake initiation at depth, shear heating produces expansion of pore fluid and an increase in pore pressure (Lachenbruch, 1980; Mase & Smith, 1984) (thermal pressurization). In fact, many of the recent studies on dynamic pore pressure changes have focused on the coseismic stage where slip has already initiated and significant frictional heat is generated (e.g., Brantut & Mitchell, 2018; Noda & Lapusta, 2013).

Surprisingly little is known on changes in pore pressure due to hydromechanical interactions during nucleation and rupture initiation. There is a practical reason for this in that pore pressure (and temperature) changes within natural rupture nucleation zones are usually inaccessible and extremely difficult to measure. Even in laboratory experiments with a precise external pore pressure control, restricted hydraulic communication with the fault may lead to discrepancies between fault zone pore pressure and the control system pressure during accelerating creep or dynamic slip. Because of their additional fluid volume, pore fluid

pressure control systems with either direct or rapid hydraulic connectivity to the fault zone generally have larger storativity than test faults, attenuating any actual pressure changes from dilatancy or compaction of the fault zone. Thus, there are virtually no direct measurements of dilatancy hardening, compaction weakening, thermal pressurization, or other phenomenon that affect pore pressure during earthquake nucleation or dynamic stress drop. For example, Segall and Rice (1995) relied on observations of pore fluid flow in fully drained velocity stepping experiments (Marone et al., 1990) to represent fault gouge dilatancy and compaction. More recent drained tests were reported for a true triaxial geometry by Samuelson et al. (2009). Alternatively, Lockner and Byerlee (1994) inferred pore pressure changes in an undrained fault from velocity-dependent changes in shear strength.

In this study we demonstrate a new experimental procedure designed to measure for the first-time pore pressure and hydromechanical interactions *during* rupture nucleation and slip. For pore pressure changes within the fault to be resolved and interpretable, the pore volume associated with the sensor needs to be small relative to the fluid volume of the fault, and volume changes of the sensor in response to pressure fluctuations need to be small relative to volume changes of the fault. In addition, response to rapid changes in pore volume will be limited by the frequency response of the sensor and the diffusivity of fluid in and out of the fault. The experiments reported here satisfy these requirements and document pore pressure effects attributable to dilation and compaction during nucleation, transient (slow) slip, and rapid slip events. We show that in some cases, premonitory dilatancy reduced pore pressure and stabilized the fault, leading to delayed instability or slow slip. In other cases, gouge compaction raised pore pressure, contributing to the onset of dynamic failure.

## 2. Experimental Methodology

The experiments were conducted at room temperature in a triaxial geometry (Brace, 1964), on 76.2 mm-diameter cylinders of Westerly granite with saw-cut fault surfaces inclined 30° to the sample axis (Figure 1). We utilize two model fault configurations, which are (1) bare surface Westerly granite and (2) a 2 mm-thick quartz gouge layer sheared between the granite forcing blocks. The sample is sufficiently large to allow the addition of a high-resolution wide-bandwidth pressure transducer to be embedded adjacent and in direct hydraulic communication with the fault zone (Figure 1), in addition to the standard external transducer. Further details of the experimental methodology can be found in the supporting information.

## 3. Experimental Results

Machine resonance time theoretically controls the duration of rapid slip events in this kind of testing apparatus (Johnson & Scholz, 1976; Shimamoto et al., 1980), a duration that is empirically found to be of order 0.1 to 10 ms (Kilgore et al., 2017; Lockner et al., 2017). While the pore pressure sensor has a much shorter resonance period, recording of fault pore pressure transients has a practical limit due to the diffusion time of fluid in the fault zone. As a consequence, pressure transients accompanying seismic slip (stick-slip) are not reliably recorded. The 100 Hz recordings of stress-stepping tests (see supporting information) indicate that the internal pore pressure transducer response is reliable at a 10 ms sampling interval. However, equilibration of fault zone pressure with the transducer may be limited to as much as a few seconds time lag, depending on diffusivity.

### 3.1. Bare Rock Surfaces

Initial experiments were conducted on flat fault surfaces roughened with #120-grit grinding compound (~106 μm grit size). Surface wear during the initial 1 to 2 mm of slip produced a fine rock powder that formed a gouge layer estimated to be approximately 30 μm thick (Lockner et al., 2017), with estimated volume of ~270 $mm^3$. Figure 2a shows shear stress and fault slip for a 0.2 μm/s loading sequence at 50 MPa confining pressure. An initial seismic stick-slip (~16 MPa stress drop) occurred at 530,371 s (Figures 2a and 2b) followed by a sequence of four smaller slow slip events. Figures 2b and 2c show the precursory accelerating slip and associated pore pressure rise before the stick-slip. A coseismic drop in pore pressure, $p$, is followed by a rapid reversal that peaks after ~10 s. The precursory rise in $p$ (0.15 MPa) reduced effective normal stress and therefore reduced fault strength by 0.11 MPa. Over the same interval, intrinsic friction rose by $\Delta\mu^{eff} = 0.005$ that corresponds to an increase in shear strength of 0.22 MPa. Thus, $\Delta p$ reduced the intrinsic strengthening in this interval by 40%. In the final second before stick-slip, $p$ began to decrease, suggesting late-stage fault

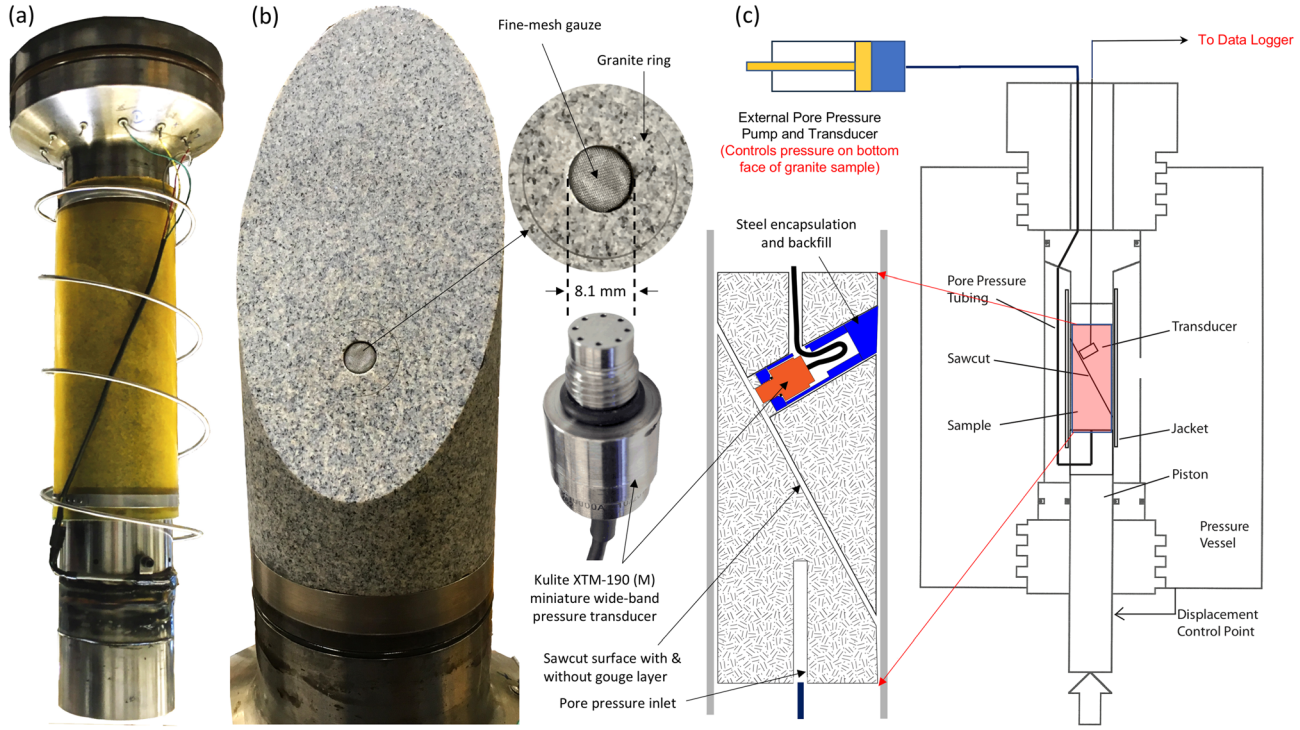


**Figure 1.** Embedded miniature pore pressure transducer and fault geometry. (a) Complete triaxial sample assembly. (b) Finished sample. The sensor has a maximum diameter larger than the active transducer face, requiring emplacement in a relatively large fault-normal borehole. A steel sleeve is epoxied into the borehole behind the transducer for support. A donut-shaped granite insert is epoxied into the front of the transducer hole and surface ground flat with the fault surface, leaving the transducer ~2 mm below the sliding surface. (c) Schematic of sample setup with embedded transducer within the triaxial sample geometry. The pressure transducer is embedded in the upper sample half, while the external pore pressure system is in communication with the base of the lower sample. The steel spacer below the sample is instrumented as an internal axial load cell.

dilation (supporting information Figure S4). Figures 3a–3d show the sequence of slow slip events that occurred with continued loading.

Unlike the earlier stick-slip case, accelerating slip before each slow slip event was accompanied by a drop in pore pressure (fault dilation) that caused a corresponding rise in $\sigma_n^{eff}$ and helped stabilize the fault. Then, each time the fault locked up, $p$ recovered. Precursory changes in $p$ were about −0.1 MPa and based on Equation 1 represent about 0.07 MPa increase in shear strength compared to a frictional weakening of about 0.2 MPa indicated by the drop in coefficient of friction ($\mu^{eff}$) (Figures 3c and 3d). During the slip events, $p$ dropped an additional ~0.1 MPa, further increasing the fault strength by 0.07 MPa, while the frictional weakening was about −0.3 MPa.

### 3.2. Quartz Gouge

Natural faults commonly contain a core of crushed gouge that contains the slip surface (e.g., Caine et al., 1996). To model this, we conducted tests on a 2 mm-thick layer of simulated quartz gouge. After shearing and compaction, gouge thickness was roughly 50 times greater than the gouge layer generated within the bare surface experiments. The median grain size of the starting material was 116 μm but undergoes rapid size reduction with shearing. The final grain size was not measured, but in a similar experiment was found to reduce to approximately 69 μm with significant production of fines. We next show a sequence of four decaying slow slip events that occurred at $P_c$ = 45 MPa and a loading rate of 10 μm/s in Figures 3e–3h. In this case, shear strength dropped during each slip event and increases between events. $p$ increased during slip (gouge compaction) and decreased between events (gouge dilation). The combination of rising $p$ and decreasing $\tau$ implies that slip is being driven by episodic gouge compaction causing reduction of $\sigma_n^{eff}$. In this example, pore pressure changes were 2 to 6 MPa, roughly 10 times larger than in the bare surface tests.

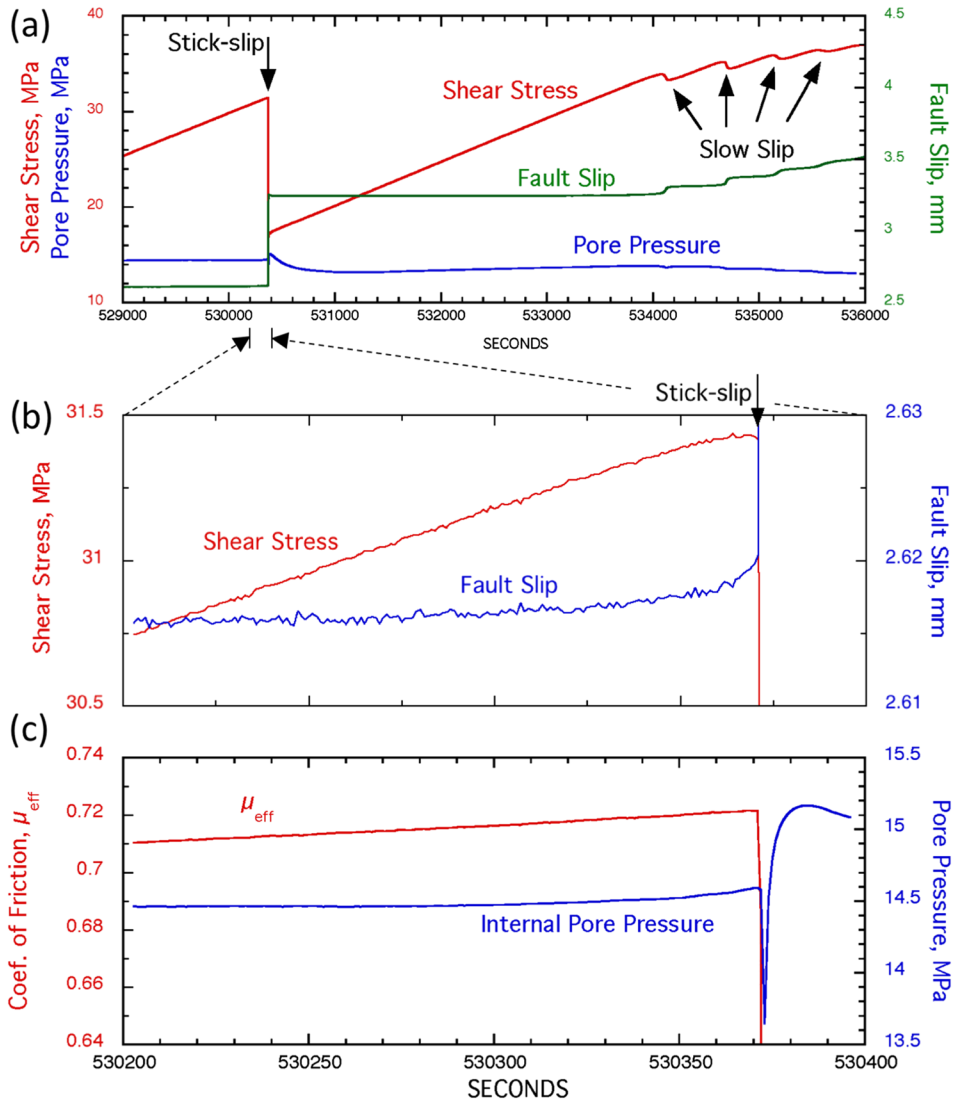


**Figure 2.** Bare surface experiment. Large seismic failure driven by shear-induced compaction. (a) Time series of shear stress and slip for large event that is followed by a sequence of creep events. (b and c) Expanded plots of shear stress, slip, pore pressure, and friction of the seismic event.

## 4. Discussion

In this study, we explore the range of hydromechanical interactions that can occur during fault deformation in hydraulically isolated faults. Fault gouge porosity and pore pressure will change with $\tau$, $\sigma_n$, mean stress, fault displacement, and sliding rate. Some variations are reversible (elastic), and others are not reversible (i.e., grain crushing or healing). Dilation will lower $p$ and, through the effective pressure law, delay or completely suppress instability. Compaction can enhance or drive slip. From poroelastic theory (Biot, 1941; Skempton, 1954), increasing mean stress will increase pore pressure in undrained conditions. In addition, increasing differential stress at constant mean stress can result in a reversible decrease in $p$ (Lockner & Beeler, 2003; Lockner & Stanchits, 2002; Skempton, 1954; Wang, 1997). Inelastic processes, such as strain- and strain rate-dependent dilatancy and shear-enhanced compaction, will also result in pore pressure transients (Scuderi et al., 2015; Segall et al., 2010; Segall & Rice, 1995). Determining the relative importance of these different effects will require systematic testing in future experiments.

Earthquake instability is often analyzed in the framework of rate- and state-dependent (RS) friction (Dieterich, 1981; Marone et al., 1990; Okubo & Dieterich, 1984; Ruina, 1983) in which second-order

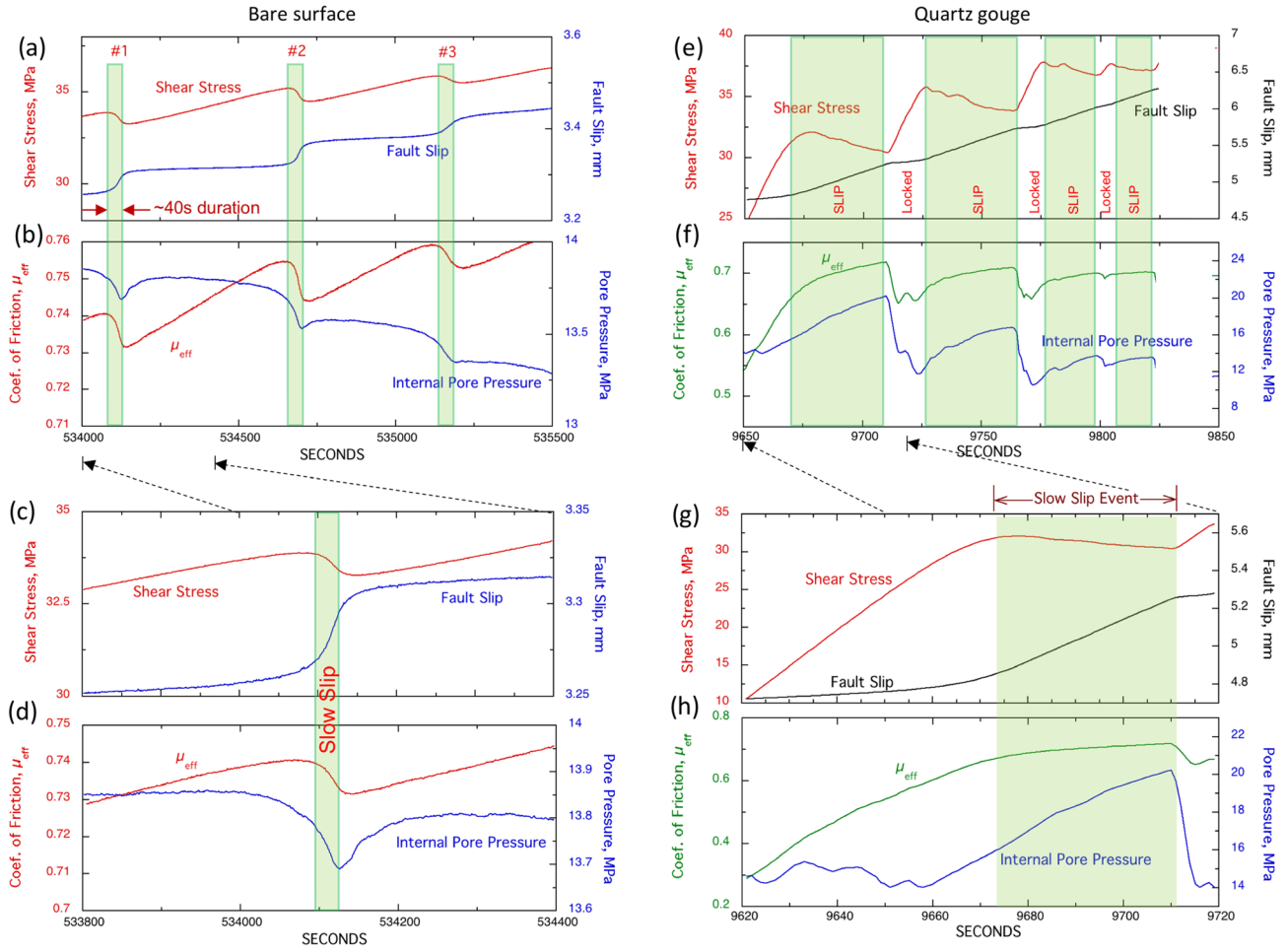


**Figure 3.** (a–d) Bare surface experiment. Sequence of creep events, stabilized by dilatancy hardening. Accelerating slip causes dilation, and decelerating slip causes compaction. The slow slip event in (c) and (d) has a duration of ~40 s. (e–h) Quartz gouge layer experiment. Sequence of four compaction-driven slip events in a fault gouge. Fault is initially locked. The onset of slip is accompanied by compaction and a large increase in pore pressure. Shear stress decreases during each slip event; however, friction continues to increase because the effective normal stress is decreasing more rapidly than shear stress. Eventually, the fault locks up, and the pattern repeats. The slow slip event in (g) and (h) has a duration of ~37 s.

strength variations can control instability. Since pore pressure has a direct effect on fault strength (Equation 1), small changes in pore volume can have a significant impact on timing and slip rate of failure (Segall et al., 2010; Segall & Rice, 1995). For the stress levels in our experiments, RS strength variations are on the order of 0.1 to 0.5 MPa. Pore pressure variations for bare surface faults (Figures 2 and 3) are of the same order, and in the case of a 2 mm gouge layer (Figure 4) are 10 times larger, suggesting that hydromechanical effects can be significant in low-permeability rocks. In addition, since gouge is ubiquitous in natural fault zones, hydromechanical effects may dominate.

### 4.1. Bare Surface Experiment

The relatively smooth, bare surface experiments were designed to reduce the characteristic friction weakening distance (Okubo & Dieterich, 1984) and enhance the likelihood of stick-slip sliding (Ruina, 1983). In our bare surface experiment the shear zone is extremely narrow and well localized, while the surrounding rock has low permeability (of order $10^{-20}$ $m^2$) such that the fault is isolated for precursory and immediate postslip timescales. For the seismic stick-slip event shown in Figure 2, failure is preceded by accelerating slip, as commonly observed under dry conditions (e.g., McLaskey & Lockner, 2014). In Figure 2, $p$ increases before instability, requiring that shear is accompanied by fault compaction. This is inconsistent with standard brittle and frictional models of failure (Brace, 1964; Segall & Rice, 1995) that involve precursory dilation, but is

not without precedent in soil mechanics (Mandl et al., 1977), and some saturated faulting tests (Faulkner et al., 2018). Relative to dry or drained tests, and in the context of the effective pressure law (Equation 1), the presence of pore fluid in this shear zone contributes to advancing the fault to failure by decreasing effective stress and therefore destabilizing fault slip. However, the (static) change in $p$ from before to immediately after seismic slip is negative, consistent with shear dilatancy. The expanded time plot (supporting information Figure S2) shows that the steady premonitory compaction reverses within 1 s of rupture and continues to dilate coseismically. While coseismic dilatancy is consistent with standard brittle and frictional failure models, the switch from compaction to dilation is an unexpected feature. The static pore pressure decrease is immediately followed by a larger postseismic, time-dependent transient increase in pore pressure (e.g., Figure 3d). This may be due to compaction associated with afterslip or from local fluid flow within the shear zone. The pore pressure increase is followed by a much slower decay that reflects a return to long-term equilibrium with the controlled external pore pressure system (1 MPa).

The subsequent slow events (Figures 3a–3d) are loaded at the same rate but undergo measurably larger premonitory creep. Apparently, the preceding seismic event modified the fault surface, making it more conducive to creep. With increasing shear stress, fault slip accelerates and $p$ decreases (implying fault dilatancy). The prior seismic event underwent a catastrophic loss of strength (16 MPa) overwhelming the stabilizing effect of a 1 MPa coseismic drop in $p$. For the slow slip events, however, a ~0.2 MPa drop in $p$ was apparently enough to maintain quasi-stable sliding (peak slip rate of ~1 μm/s) with a smaller shear strength loss of about 0.1 MPa. Shortly after the peak slip rate, $p$ begins to increase, presumably as reduced slip rate leads to fault compaction. These collective observations of pore pressure change accompanying precursory and peak slip velocities are consistent with standard dilatancy hardening and increasing effective stress during failure (Rice & Rudnicki, 1979; Segall et al., 2010; Segall & Rice, 1995) producing prolonged precursors and stabilizing slip, relative to dry or drained tests.

### 4.2. Gouge Experiment

The 2 mm gouge example shown in Figures 3e–3h demonstrates slip oscillations that are apparently driven by a coupling of slip rate-dependent pore volume and pore pressure-dependent strength. In the first cycle of accelerated slip (9,670 to 9,710 s), $p$ rose by 4.8 MPa, causing a strength loss (Equation 1) of ~3.4 MPa. Over this same interval, the 0.06 increase in $\mu^{eff}$ implies strengthening due to intrinsic friction of 2.8 MPa. Thus, the overall weakening of the fault during the slip event is the result of gouge compaction and increasing $p$ dominating the frictional strengthening. Following the end of the slip event, the fault locked up and a corresponding dilation and drop in $p$ followed as the fault continued to load. The 6 MPa decrease in $p$ during lockup corresponds to a 4.2 MPa increase in shear strength and accounts for most of the observed 5 MPa strength rise before the onset of the next slip event. This sequence of lockup (dilatancy) and slip (compaction) happened three more times with diminishing amplitude before deformation returned to stable sliding. We note that this sequence in which increase in slip rate corresponds to gouge compaction is the opposite of the response assumed in the Segall and Rice (1995) model. The cycling of lockup and release is also reminiscent of force chain models that support boundary tractions in deformation of granular materials (Daniels & Hayman, 2008; Mair & Hazzard, 2007; Peters et al., 2005) and produce cyclic variations in dilatancy/compaction.

### 4.3. Pore Pressure Transients and Intrinsic Friction

Segall and Rice (1995) developed constitutive equations combining RS friction, log (velocity)-dependent gouge dilatancy, gouge/fluid compressibility, and diffusion in fault-bounding rock. They assumed a positive dilatancy coefficient based on drained deformation tests (Marone et al., 1990) such that increased slip rate would reduce pore pressure. They noted that this model assumed a fully developed gouge layer and that rapidly evolving gouge structure, especially during initial shearing, would likely involve volume change not accounted for in their model. The three examples that we present here show transient response associated with initial loading or reloading of the fault and may not be directly applicable to the Segall and Rice model. We note, however, that Segall and Rice (1995) obtained the dilatancy coefficient that they used in their model from triaxial laboratory tests (Marone et al., 1990) performed under similar conditions to the ones reported here. In our examples, stick-slip (Figure 2b) occurs after 2.6 mm slip on the bare fault surface with fully developed strength ($\mu^{eff} = 7.1$). Even so, accelerating premonitory creep is accompanied by increasing $p$. Coseismic and postseismic slip are accompanied by,

respectively, a drop and then increase in $p$, both qualitatively consistent with the Segall and Rice model. In the bare surface slow slip sequence (Figures 3a–3d) the transient accelerating/decelerating sequences are associated with decreasing/increasing variations in $p$. This response is also qualitatively in agreement with Segall and Rice. Transients in the gouge slow slip sequence (Figures 3e–3h), however, are slip rate related but are opposite in sign to Segall and Rice model predictions: Increased slip rate is associated with increased $p$. In this initial study, we cannot identify the fault properties controlling this wide range of pore pressure response. We do not have direct measurements of gouge compaction or grain size evolution for these experiments. Additional tests will be needed to address the issue of fault evolution and when it is appropriate to apply the Segall and Rice model to natural and laboratory faults.

We briefly consider the relative importance of pore pressure transients and RS frictional variations in controlling fault stability. Prior to stick-slip (Figure 2), transient rise in $p$ is about 0.16 MPa (implying 0.1 MPa shear strength loss), while the friction coefficient is nearly constant (Figure 2c). This implies that $p$ increase is at least a contributing factor in determining timing and onset of instability. Then, in Figure 3d, the drop in $p$ during slow slip increases fault strength by about 0.1 MPa, while the intrinsic RS weakening (based on $\mu^{eff}$) is 0.4 MPa. Thus, the $p$ transient reduces the magnitude of the intrinsic frictional weakening by about 25%. In these two examples, increasing pore pressure enhanced instability before stick slip and then partially suppressed the intrinsic weakening when slow slip occurred. The modification of strengthening or weakening by $p$ may be important in determining dynamic failure versus quasi-stable slip by modifying the rate of strength loss compared to the unloading stiffness. In the gouge example (Figures 3g and 3h), frictional strength increases during slow slip ($\mu^{eff}$ increases) by about 2.8 MPa, while the rise in $p$ decreases shear strength by ~3.4 MPa. In this case, gouge compaction and rise in $p$ dominates the frictional strength increase and drives the instability.

### 4.4. Frictional Heating

Recent experimental work has focused on coseismic heating of faults (Di Toro et al., 2011), with focus on seeing pressure changes due to frictional heating (Brantut & Mitchell, 2018). We show similar pressure changes, without including heat, and it is possible that dilation and pressure drop might buffer thermal pressurization. Still, the stick-slip event shown in Figure 2 involved a 50% stress drop and presents the possibility that frictional heating may have contributed to dynamic strength loss. While we do not have precise measurement of important variables such as coseismic pore pressure, volume change, frictional work, or temperature, we can provide some constraints. We show with a simple 1-D heat flow calculation that peak fault zone temperature rise could exceed 100°C (see supporting information). This presents the possibility that thermal pressurization during the short but energetic slip event might have contributed to dynamic weakening and the relatively large stress drop. This effect will be explored in future experiments.

## 5. Conclusions

We have measured pore pressure transients in hydraulically isolated laboratory faults during seismic and slow slip events. A novel feature of these experiments is the use of a miniature pressure transducer embedded in the sample adjacent to the fault surface. We observed a variety of pore pressure transients corresponding to precursory, coseismic, and postseismic deformation. Hydraulic isolation causes time- and slip-dependent changes in pore volume to generate pore pressure transients from 0.1 to >10 MPa. Under some circumstances these transients dominate and control both failure time and stability. Both increasing pore pressure (compaction) and decreasing pressure (dilation) can occur as precursors and coseismically. Our observations are not definitive, but they present the possibility that during the immediate precursory period, dilation delays stick-slip and may lead to slow slip in faults that are rate or slip weakening, that is, faults that would fail seismically under drained or dry conditions. Conversely, compaction destabilizes rate- or slip-weakening faults and can also lead to an accelerated preparation phase. For rate- or slip-strengthening faults, compaction may produce slow events that have no dry or drained analog. These experiments demonstrate the importance of pore fluid-rock interactions in controlling slip instability in hydraulically isolated faults. The granular shear zones simulated and evolved in these experiments are similar to the expected state of natural fault cores. It is important to note that our experiments represent an end-member case where the fault is hydraulically isolated. In nature, fault gouge zones can be tens of

centimeters wide and slip can localize in narrower principal slip zones within the low-permeability gouge zone, meaning the active slip zone is hydraulically isolated. However, slip can also localize on the boundaries of the fault core adjacent to a more permeable fracture damage zone (Mitchell & Faulkner, 2009), which can change both permeability and storativity and therefore shorten the diffusivity time constant. Our experiments demonstrate, for the first time, not only that fluids play a significant role in controlling fluid-saturated fault behavior but that in some instances hydromechanical effects may be the dominant mechanisms in controlling fault stability. These processes are just as important, if not more so, than commonly invoked mechanisms such as RS friction. The currently accepted hydromechanical model for fault zone stability (Segall & Rice, 1995) assumes only rate-dependent dilatancy leading to instability. Here, we demonstrate the importance of both dilatancy *and* compaction/pore collapse during nucleation and rapid slip leading to instability. Hydraulically isolated saturated gouge experiments have been reported for decades by many authors focusing on rate and state parameters. We note that many such experiments may actually be measuring dominant poromechanical effects rather than the empirical constitutive parameters such as RS ($a$ and $b$) (Brace & Martin, 1968; Morrow et al., 2017; Raleigh & Paterson, 1965; Schmitt & Zoback, 1992). Our experiments also suggest alternative and more physically meaningful definitions of fault "state." In RS friction formulations, state is usually either a dimensionless quantity or, equivalently, has temporal units (age) (Ruina, 1983). The age dependence is thought to represent the time-dependent growth of contact area (the age of the asperity population) or equivalently an inverse dependence of the asperity population on slip speed (i.e., inversely proportional to age). Implicitly, a change in contact area implies dilatancy or compaction. Thus, it is relatively straightforward to modify the existing RS framework to cast "state" as porosity or degree of dilatancy relative to a reference state as developed in Segall and Rice (1995). This is a familiar concept in soil mechanics where overconsolidated or underconsolidated materials have different rheological behavior compared to porosity attained in fully developed shear flow. Our saturated tests indicate that stress-dilatancy relations are incompletely represented in existing fault constitutive relations. In other words, in order for us to truly make comprehensive models of fault behavior leading to earthquake instability, we need to understand the fundamental conditions that lead to both dilatant and compactive behavior. This will require further experiments to identify the conditions leading to these radically different behaviors, including confined measurements of fault dilation and stress state that cover the range of crustal temperatures and effective stresses of in situ fault slip.

## Data Availability Statement

Data for Figures 2 and 3 can be found at https://doi.org/10.5066/P98U3DZX (Figure 1 has no data). This doi number has been set aside for this data release by the USGS online repository. It will not go active until it has passed internal USGS review. In the meantime, we have uploaded the dataset in the supporting information and will confirm the DOI once the paper is accepted/revised.

**Acknowledgments**

T. M. M. acknowledges support from the UK Natural Environmental Research Council Grant NE/M004716/1. We thank Andy Barbour, J. Ole Kaven, Marcus Scuderi, and an anonymous reviewer for constructive comments that improved the manuscript. Any use of trade, firm, or product names is for descriptive purposes only and does not imply endorsement by the U.S. government.

## References

Biot, M. A. (1941). General theory of three-dimensional consolidation. *Journal of Applied Physics*, *12*(2), 155–164. https://doi.org/10.1063/1.1712886

Brace, W. F. (1964). Brittle fracture of rocks. In W. R. Judd (Ed.), *State of stress in the Earth's crust* (pp. 110–178). New York, New York: Elsevier.

Brace, W. F., & Martin, R. J. (1968). A test of law of effective stress for crystalline rocks of low porosity. *International Journal of Rock Mechanics and Mining Sciences*, *5*(5), 415. https://doi.org/10.1016/0148-9062(68)90045-4

Brantut, N. (2020). Dilatancy-induced fluid pressure drop during dynamic rupture: Direct experimental evidence and consequences for earthquake dynamics. *Earth and Planetary Science Letters*, *538*, 116179. https://doi.org/10.1016/j.epsl.2020.116179

Brantut, N., & Mitchell, T. M. (2018). Assessing the efficiency of thermal pressurization using natural pseudotachylyte-bearing rocks. *Geophysical Research Letters*, *45*, 9533–9541. https://doi.org/10.1029/2018GL078649

Caine, J. S., Evans, J. P., & Forster, C. B. (1996). Fault zone architecture and permeability structure. *Geology*, *24*(11), 1025–1028. https://doi.org/10.1130/0091-7613(1996)024<1025:FZAAPS>2.3.CO;2

Daniels, K. E., & Hayman, N. W. (2008). Force chains in seismogenic faults visualized with photoelastic granular shear experiments. *Journal of Geophysical Research*, *113*, B11411. https://doi.org/10.1029/2008jb005781

Di Toro, G., Han, R., Hirose, T., De Paola, N., Nielsen, S., Mizoguchi, K., et al. (2011). Fault lubrication during earthquakes. *Nature*, *471*(7339). https://doi.org/10.1038/nature09838

Dieterich, J. H. (1981). Constitutive properties of faults with simulated gouge. In *Mechanical behavior of crustal rocks*, *Geophysical Monograph Series* (24, 103–120). Washington, DC: American Geophysical Union. https://doi.org/10.1029/GM024p0103

Faulkner, D. R., Sanchez-Roa, C., Boulton, C., & den Hartog, S. A. M. (2018). Pore fluid pressure development in compacting fault gouge in theory, experiments, and nature. *Journal of Geophysical Research: Solid Earth*, *123*, 226–241. https://doi.org/10.1002/2017jb015130

Hubbert, M. K., & Rubey, W. W. (1959). Role of fluid pressure in mechanics of overthrust faulting.1. Mechanics of fluid-filled porous solids and its application to overthrust faulting. *Geological Society of America Bulletin*, *70*(2), 115–166. https://doi.org/10.1130/0016-7606(1959)70[115:ROFPIM]2.0.CO;2

Johnson, T. L., & Scholz, C. H. (1976). Dynamic properties of stick-slip friction of rock. *Journal of Geophysical Research*, *81*(5), 881–888. https://doi.org/10.1029/JB081i005p00881

Kilgore, B. D., McGarr, A., Beeler, N. M., & Lockner, D. A. (2017). *Earthquake source properties from instrumented laboratory stick-slip*, *Geophysical Monography Series* (Vol. 227, pp. 151–169). Washington, DC, and Hoboken, NJ: American Geophysical Union and John Wiley and Sons, Inc. https://doi.org/10.1002/9781119156895

Lachenbruch, A. H. (1980). Frictional heating, fluid pressure, and the resistance to fault motion. *Journal of Geophysical Research*, *85*(B11), 6097–6112. https://doi.org/10.1029/JB085iB11p06097

Lockner, D. A., & Beeler, N. M. (2003). The shearing resistance of saturated soils (pp. 54–56). Paper presented at Proceedings of the 1st International Conference on Soil Mechanics and Foundation Engineering.

Lockner, D. A., & Byerlee, J. D. (1994). Dilatancy in hydraulically isolated faults and the suppression of instability. *Geophysical Research Letters*, *21*(22), 2353–2356. https://doi.org/10.1029/94gl02366

Lockner, D. A., Kilgore, B. D., Beeler, N. M., & Moore, D. E. (2017). *The transition from frictional sliding to shear melting in laboratory stick-slip experiments*, *Geophysical Monography Series* (Vol. 227, pp. 105–131). Washington, DC, and Hoboken, NJ: American Geophysical Union and John Wiley and Sons, Inc. https://doi.org/10.1002/9781119156895

Lockner, D. A., & Stanchits, S. A. (2002). Undrained poroelastic response of sandstones to deviatoric stress change. *Journal of Geophysical Research*, *107*(B12), 2353. https://doi.org/10.1029/2001jb001460

Mair, K., & Hazzard, J. F. (2007). Nature of stress accommodation in sheared granular material: Insights from 3D numerical modeling. *Earth and Planetary Science Letters*, *259*(3–4), 469–485. https://doi.org/10.1016/j.epsl.2007.05.006

Mandl, G., De Jong, L. N. J., & Maltha, A. (1977). Shear zones in granular materials. *Rock Mechanics*, *9*(2-3), 95–144. https://doi.org/10.1007/BF01237876

Marone, C., Raleigh, C. B., & Scholz, C. H. (1990). Frictional behavior and constitutive modeling of simulated fault gouge. *Journal of Geophysical Research*, *95*(B5), 7007–7025. https://doi.org/10.1029/JB095iB05p07007

Mase, C. W., & Smith, L. (1984). Pore-fluid pressures and frictional heating on a fault surface. *Pure and Applied Geophysics*, *122*(2–4), 583–607.

McLaskey, G. C., & Lockner, D. A. (2014). Preslip and cascade processes initiating laboratory stick slip. *Journal of Geophysical Research: Solid Earth*, *119*, 6323–6336. https://doi.org/10.1002/2014jb011220

Mitchell, T. M., & Faulkner, D. R. (2009). The nature and origin of off-fault damage surrounding strike-slip fault zones with a wide range of displacements: A field study from the Atacama fault system, northern Chile. *Journal of Structural Geology*, *31*(8), 802–816. https://doi.org/10.1016/j.jsg.2009.05.002

Morrow, C. A., Moore, D. E., & Lockner, D. A. (2017). Frictional strength of wet and dry montmorillonite. *Journal of Geophysical Research: Solid Earth*, *122*, 3392–3409. https://doi.org/10.1002/2016jb013658

Noda, H., & Lapusta, N. (2013). Stable creeping fault segments can become destructive as a result of dynamic weakening. *Nature*, *493*(7433), 518–521. https://doi.org/10.1038/nature11703

Okubo, P. G., & Dieterich, J. H. (1984). Effects of physical fault properties on frictional instabilities produced on simulated faults. *Journal of Geophysical Research*, *89*(Nb7), 5817–5827. https://doi.org/10.1029/JB089iB07p05817

Peters, J. F., Muthuswamy, M., Wibowo, J., & Tordesillas, A. (2005). Characterization of force chains in granular material. *Physical Review E*, *72*(4). https://doi.org/10.1103/PhysRevE.72.041307

Raleigh, C. B., & Paterson, M. S. (1965). Experimental deformation of serpentinite and its tectonic implications. *Journal of Geophysical Research*, *70*(16), 3965. https://doi.org/10.1029/JZ070i016p03965

Rice, J. R., & Rudnicki, J. W. (1979). Earthquake precursory effects due to pore fluid stabilization of a weakening fault zone. *Journal of Geophysical Research*, *84*(Nb5), 2177–2193. https://doi.org/10.1029/JB084iB05p02177

Ruina, A. (1983). Slip instability and state variable friction laws. *Journal of Geophysical Research*, *88*(B12), 10,359–10,370. https://doi.org/10.1029/JB088iB12p10359

Samuelson, J., Elsworth, D., & Marone, C. (2009). Shear-induced dilatancy of fluid-saturated faults: Experiment and theory. *Journal of Geophysical Research*, *114*, B12404. https://doi.org/10.1029/2008jb006273

Schmitt, D. R., & Zoback, M. D. (1992). Diminished pore pressure in low-porosity crystalline rock under tensional failure—Apparent strengthening by dilatancy. *Journal of Geophysical Research*, *97*(B1), 273–288. https://doi.org/10.1029/91jb02256

Scuderi, M. M., Carpenter, B. M., Johnson, P. A., & Marone, C. (2015). Poromechanics of stick-slip frictional sliding and strength recovery on tectonic faults. *Journal of Geophysical Research: Solid Earth*, *120*, 6895–6912. https://doi.org/10.1002/2015jb011983

Segall, P., & Rice, J. R. (1995). Dilatancy, compaction, and slip instability of a fluid-infiltrated fault. *Journal of Geophysical Research*, *100*(B11), 22,155–22,171. https://doi.org/10.1029/95jb02403

Segall, P., Rubin, A. M., Bradley, A. M., & Rice, J. R. (2010). Dilatant strengthening as a mechanism for slow slip events. *Journal of Geophysical Research*, *115*, B12305. https://doi.org/10.1029/2010jb007449

Shimamoto, T., Handin, J., & Logan, J. M. (1980). Specimen-apparatus interaction during stick-slip in a triaxial compression machine—A decoupled 2-degree-of-freedom model. *Tectonophysics*, *67*(3–4), 175–205. https://doi.org/10.1016/0040-1951(80)90234-6

Skempton, A. W. (1954). The pore pressure coefficients *A* and *B*. *Geotechnique*, *4*(4), 143–147. https://doi.org/10.1680/geot.1954.4.4.143

Stanchits, S. A., Lockner, D. A., & Ponomarev, A. V. (2003). Anisotropic changes in *P*-wave velocity and attenuation during deformation and fluid infiltration of granite. *Bulletin of the Seismological Society of America*, *93*(4), 1803–1822. https://doi.org/10.1785/0120020101

Terzaghi, K. (1936). The shearing resistance of saturated soils, Proc. 1st Int. Conf. Soil Mech., 1, 54–56.

Wang, H. F. (1997). Effects of deviatoric stress on undrained pore pressure response to fault slip. *Journal of Geophysical Research*, *102*(B8), 17,943–17,950. https://doi.org/10.1029/97jb01358